Journal of Modern Optics
Vol. 53, Nos. 5–6, 20 March–15 April 2006, 699–711

Taylor & Francis
Taylor & Francis Group

Quantum parallel dense coding of optical images

T. YU. GOLUBEVA†, YU. M. GOLUBEV†,
I. V. SOKOLOV*† and M. I. KOLOBOV‡

†V.A. Fock Physics Institute, St Petersburg State University,
198504 Petrodvorets, St Petersburg, Russia
‡Laboratoire PhLAM, Université de Lille-1,
F-59655 Villeneuve d'Ascq cedex, France

(*Received 27 January 2005; in final form 24 May 2005*)

We propose quantum dense coding protocol for optical images. This protocol extends the earlier proposed dense coding scheme for continuous variables [S.L. Braunstein and H.J. Kimble, Phys. Rev. A **61** 042302 (2000)] to an essentially multimode in space and time optical quantum communication channel. This new scheme allows, in particular, for parallel dense coding of non-stationary optical images. Similar to some other quantum dense coding protocols, our scheme exploits the possibility of sending a message through only one of the two entangled spatially-multimode beams, using the other one as a reference system. We evaluate the Shannon mutual information for our protocol and find that it is superior to the standard quantum limit. Finally, we show how to optimize the performance of our scheme as a function of the spatio-temporal parameters of the multimode entangled light and of the input images.

1. Introduction

The fundamental properties and possible applications of non-classical light have been extensively investigated starting from the mid 1970s. In the past decade, novel fields of application of non-classical light have emerged, such as quantum information [1, 2] and quantum imaging [3, 4]. Quantum imaging uses spatially multimode non-classical states of light with quantum fluctuations suppressed not only in time, but also in space. The promising idea is to introduce optical parallelism inherent in quantum imaging into various protocols of quantum information, such as quantum teleportation, quantum dense coding, quantum cryptography etc., thus increasing their information possibilities. The continuous variables quantum teleportation protocol proposed in [5, 6] and experimentally realized in [7, 8] has been recently extended for teleportation of optical images in [9, 10].

Quantum dense coding was first proposed and experimentally realized for discrete variables, *qubits* [11, 12], and later generalized and experimentally realized for continuous variables in [13, 14]. In this paper we propose the continuous

*Corresponding author. Email: sokolov@is2968.spb.edu

Journal of Modern Optics
ISSN 0950–0340 print/ISSN 1362–3044 online
http://www.tandf.co.uk/journals
DOI: 10.1080/09500340500217506

variables quantum dense coding protocol for optical images. Our scheme extends the protocol [13] to the essentially multimode in space and time optical communication channel. This generalization exploits the inherent parallelism of optical communication and allows for simultaneous parallel dense coding of an input image with N elements. In the case of a single spatial mode considered in [13] one has $N = 1$.

We calculate the Shannon mutual information for a stream of classical input images in a coherent state. In this paper we assume arbitrarily large transverse dimensions of propagating light beams and an unlimited spatial resolution for the photodetection scheme. That is, we actually find an upper bound on the spatio-temporal *density* of the information stream in bits per cm^2 s. This density depends on the degree of squeezing and entanglement in non-classical illuminating light. Two sets of spatio-temporal parameters play an important role in our protocol: (i) the coherence length and the coherence time of spatially-multimode squeezing and entanglement and (ii) the spatio-temporal parameters of the stream of input images. In our analysis we assume that the sender (Alice) produces a uniform ensemble of images with the Gaussian statistics, characterized by a certain resolution in space and time (the Alice grain).

We demonstrate that the essentially multimode quantum communication channel provides much higher channel capacity than a single-mode quantum channel due to its intrinsic parallel nature. The density of the information stream is in particular limited by diffraction. We find that the role of diffraction can be partially compensated by lenses properly inserted in the scheme. An important difference between the classical communication channel (i.e. with vacuum fluctuations at the input of the scheme instead of multimode entangled light) and its quantum counterpart is that in the quantum case there exists an optimum spatial density of the signal image elements, which should be matched with the spatial frequency band of entanglement.

In section 2 we describe in detail the scheme for the dense coding protocol for optical images. The channel capacity of our communication scheme is evaluated in section 3. We make our conclusions in section 4. The relevant details for our analysis properties of spatially-multimode squeezing are given in the Appendix.

2. Spatially-multimode quantum dense coding channel

The optical scheme implementing the protocol is shown in figure 1. Compared to the generic continuous variables dense coding scheme [13], here the light fields are assumed to be spatially multimode. At the input, the spatially-multimode squeezed light beams, with the slow field amplitudes $S_1(\boldsymbol{\rho}, t)$ and $S_2(\boldsymbol{\rho}, t)$ in the Heisenberg representation, are mixed at the symmetrical beamsplitter BS_1. For a properly chosen orientation of the squeezing ellipses of the input fields, the scattered fields $E_1(\boldsymbol{\rho}, t)$ and $E_2(\boldsymbol{\rho}, t)$ are in the entangled state with correlated field quadrature components, as illustrated in figure 1.

The classical signal image field $A(\boldsymbol{\rho}, t)$ is created by Alice in the first beam by means, e.g. of the controlled (with given resolution in space–time) mixing device Mod with almost perfect transmission for the non-classical field $E_1(\boldsymbol{\rho}, t)$.

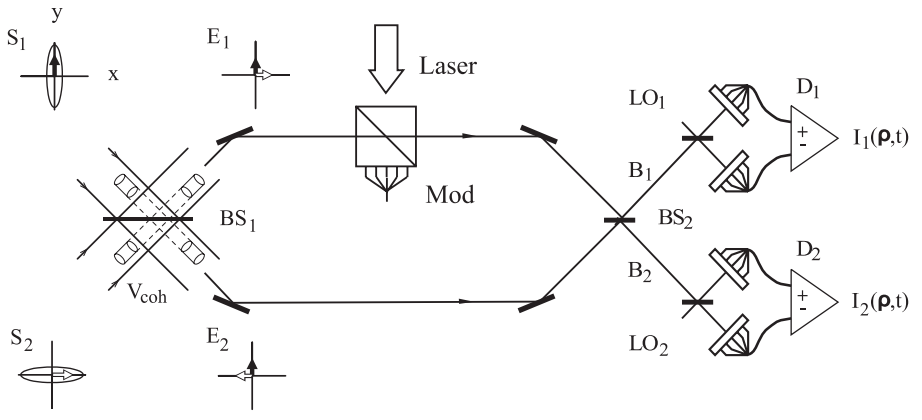

Figure 1. Optical scheme for spatially-multimode dense coding.

The receiver (Bob) detects the entangled state of two beams by means of optical mixing on the symmetrical output beamsplitter BS_2 and the homodyne detection of quadrature components of the output fields $B_1(\boldsymbol{\rho}, t)$ and $B_2(\boldsymbol{\rho}, t)$. This allows for measurement of both quadrature components of the image field with effective quantum noise reduction.

One can give a more straightforward explanation of the sub-shot-noise detection of the signal in the scheme shown in figure 1. For the symmetrical scattering matrix of the beamsplitters

$$\{R_{nm}\} = \frac{1}{2^{1/2}} \begin{pmatrix} 1 & 1 \\ 1 & -1 \end{pmatrix} \tag{1}$$

and equal optical paths of two beams, the effective Mach–Zehnder interferometer directs the input squeezed field $S_1(\boldsymbol{\rho}, t)$ onto the detector D_1, and similarly for $S_2(\boldsymbol{\rho}, t)$, thus allowing for sub-shot-noise detection of the squeezed quadrature components in both beams.

The fields at the inputs of the homodyne detectors D_1 and D_2 are

$$B_n(\boldsymbol{\rho}, t) = S_n(\boldsymbol{\rho}, t) + \frac{1}{2^{1/2}} A(\boldsymbol{\rho}, t), \tag{2}$$

where $n = 1, 2$. In the paraxial approximation, the slow amplitude of light field $B_n(\boldsymbol{\rho}, t)$ is related to the creation and annihilation operators $b_n^{\dagger}(\mathbf{q}, \Omega)$ and $b_n(\mathbf{q}, \Omega)$ for the plane waves with the transverse component of the wave vector $\mathbf{q}$ and frequency Ω given by

$$B_n(\boldsymbol{\rho}, t) = \frac{1}{(L^2 T)^{1/2}} \sum_{\mathbf{q}, \Omega} b_n(\mathbf{q}, \Omega) \exp[\mathrm{i}(\mathbf{q} \cdot \boldsymbol{\rho} - \Omega t)]. \tag{3}$$

In the case of large quantization volume with the transverse and longitudinal dimensions L and cT, the summation is performed over the following values of $\mathbf{q}$ and Ω: $\mathbf{q} = (q_x, q_y)$, $q_x = (2\pi/L)n_x$, $q_y = (2\pi/L)n_y$ and $\Omega = (2\pi/T)n$ with n_x, n_y and n taking the values 0, ± 1, ± 2, ...

The free-field commutation relations are given by

$$\Big[B_n(\boldsymbol{\rho}, t), B^{\dagger}_{n'}(\boldsymbol{\rho}', t')\Big] = \delta_{n,n'}\delta(\boldsymbol{\rho} - \boldsymbol{\rho}')\,\delta(t - t')\,,$$
$$\Big[b_n(\mathbf{q}, \Omega), b^{\dagger}_{n'}(\mathbf{q}', \Omega')\Big] = \delta_{n,n'}\,\delta_{\mathbf{q},\mathbf{q}'}\,\delta_{\Omega,\Omega'}. \tag{4}$$

The value of the irradiance (in photons per $\mathrm{cm}^2\mathrm{s}$) is equal to $B^{\dagger}_n(\boldsymbol{\rho}, t)B_n(\boldsymbol{\rho}, t)$ and the number of photons in the field mode $(\mathbf{q}, \Omega)$, localized in the quantization volume L^2cT, is $b^{\dagger}_n(\mathbf{q}, \Omega)b_n(\mathbf{q}, \Omega)$. The observed photocurrent densities,

$$I_1(\boldsymbol{\rho}, t) = B_0\Big[B_1(\boldsymbol{\rho}, t) + B^{\dagger}_1(\boldsymbol{\rho}, t)\Big],$$
$$I_2(\boldsymbol{\rho}, t) = B_0\,\frac{1}{\mathrm{i}}\Big[B_2(\boldsymbol{\rho}, t) - B^{\dagger}_2(\boldsymbol{\rho}, t)\Big], \tag{5}$$

have the following Fourier amplitudes

$$i_1(\mathbf{q}, \Omega) = B_0\Big[b_1(\mathbf{q}, \Omega) + b^{\dagger}_1(-\mathbf{q}, -\Omega)\Big],$$
$$i_2(\mathbf{q}, \Omega) = B_0\,\frac{1}{\mathrm{i}}\Big[b_2(\mathbf{q}, \Omega) - b^{\dagger}_2(-\mathbf{q}, -\Omega)\Big], \tag{6}$$

where B_0 (taken as real) and $\mathrm{i}B_0$ are the local oscillator amplitudes used in the homodyne detection (see the discussion in subsection 3.2). Here and in what follows we denote the Fourier amplitudes of the fields and the photocurrent densities by the lower-case symbols.

The squeezing transformation performed by the optical parametric amplifiers (the OPAs), illuminating the inputs of the scheme, can be written [3] as follows:

$$s_n(\mathbf{q}, \Omega) = U_n(\mathbf{q}, \Omega)c_n(\mathbf{q}, \Omega) + V_n(\mathbf{q}, \Omega)c^{\dagger}_n(-\mathbf{q}, -\Omega), \tag{7}$$

where the coefficients $U_n(\mathbf{q}, \Omega)$ and $V_n(\mathbf{q}, \Omega)$ depend on the pump-field amplitudes of the OPAs, their nonlinear susceptibilities and the phase-matching conditions (see Appendix for definitions of the squeezing parameters). The input fields $c_n(\mathbf{q}, \Omega)$ of the OPAs are assumed to be in the vacuum state.

After some calculation we obtain for the Fourier amplitudes of the photocurrent densities:

$$i_n(\mathbf{q}, \Omega) = B_0\big\{f_n(\mathbf{q}, \Omega) + a_n(\mathbf{q}, \Omega)\big\}, \tag{8}$$

where

$$f_1(\mathbf{q}, \Omega) = \Big[\exp[r_1(\mathbf{q}, \Omega)]\cos\psi_1(\mathbf{q}, \Omega)$$
$$+ \mathrm{i}\exp[-r_1(\mathbf{q}, \Omega)]\sin\psi_1(\mathbf{q}, \Omega)\Big]\exp[-\mathrm{i}\phi_1(\mathbf{q}, \Omega)]c_1(\mathbf{q}, \Omega)$$
$$+ [h.c., (\mathbf{q}, \Omega) \to (-\mathbf{q}, -\Omega)], \tag{9}$$

and

$$f_2(\mathbf{q},\Omega) = \Big[\exp[-r_2(\mathbf{q},\Omega)]\cos\psi_2(\mathbf{q},\Omega) + \mathrm{i}\exp[r_2(\mathbf{q},\Omega)]\sin\psi_2(\mathbf{q},\Omega)\Big]\exp[-\mathrm{i}\phi_2(\mathbf{q},\Omega)]c_2(\mathbf{q},\Omega) + [h.c., (\mathbf{q},\Omega)\to(-\mathbf{q},-\Omega)], \tag{10}$$

represent the quantum fluctuations of the fields at both photodetectors, and

$$a_1(\mathbf{q},\Omega) = \frac{1}{2^{1/2}}\Big[a(\mathbf{q},\Omega) + a^*(-\mathbf{q},-\Omega)\Big],$$
$$a_2(\mathbf{q},\Omega) = \frac{1}{\mathrm{i}2^{1/2}}\Big[a(\mathbf{q},\Omega) - a^*(-\mathbf{q},-\Omega)\Big], \tag{11}$$

are the components of the Alice signal image detected by Bob. Here $a(\mathbf{q},\Omega)$ is the Fourier transform of classical field $A(\boldsymbol{\rho},t)$, defined in analogy to (3).

3. Channel capacity

3.1 *Degrees of freedom of the noise and the image field*

In order to estimate the channel capacity one has to define the degrees of freedom of the noise and the signal in our spatially-multimode scheme.

We shall assume that all elements of the scheme, the OPA nonlinear crystals, beamsplitters, modulator and the CCD matrices of the detectors, have large transverse dimensions. The squeezed light fields are random variables which are stationary in time and uniform over the cross-section of the beams. That is, all correlation functions of these fields are translationally invariant in the $\boldsymbol{\rho}, t$ space. For the observed photocurrent densities this implies that any pair of Fourier amplitudes (9) and (10) for given $(\mathbf{q},\Omega)$ and $(-\mathbf{q},-\Omega)$ result from squeezing of the input fields $c(\mathbf{q},\Omega)$ and $c(-\mathbf{q},-\Omega)$ and therefore is independent of any other pair.

On the other hand, since the observed photocurrent densities are real the Fourier amplitudes $i_n(\mathbf{q},\Omega)$ and $i_n^\dagger(-\mathbf{q},-\Omega)$ are not independent, where

$$i_n(\mathbf{q},\Omega) = i_n^\dagger(-\mathbf{q},-\Omega). \tag{12}$$

For this reason we consider as independent random variables only the noise terms in Fourier amplitudes $i_n(\mathbf{q},\Omega)$ for $\Omega > 0$. The real and imaginary parts of the complex amplitudes $i_n(\mathbf{q},\Omega)$ for $\Omega > 0$ are related to the amplitudes of the real photocurrent noise harmonics $\sim\cos(\mathbf{q}\cdot\boldsymbol{\rho} - \Omega t)$ and $\sim\sin(\mathbf{q}\cdot\boldsymbol{\rho} - \Omega t)$, directly recovered by Bob from his measurements.

The Fourier amplitudes of the photocurrent densities (8) satisfy relation (12) and therefore it is sufficient to take into account only $\Omega > 0$. The random signal sent by Alice is assumed to be stationary and uniform in the cross-section of the beams. The amplitudes $a_n(\mathbf{q},\Omega)$ for $\Omega > 0$, $n = 1, 2$, are taken as independent complex Gaussian variables with variance $\sigma^{\mathrm{A}}(\mathbf{q},\Omega)$ depending on $(\mathbf{q},\Omega)$. Since transformation (11) is unitary, the Fourier classical amplitudes $a(\mathbf{q},\Omega)$ for any $(\mathbf{q},\Omega)$ are also statistically independent and the quantity

$$\sigma^{\mathrm{A}}(\mathbf{q},\Omega) = \langle|a(\mathbf{q},\Omega)|^2\rangle \tag{13}$$

is the mean photon number in the Alice signal wave $(\mathbf{q}, \Omega)$ in the quantization volume, where $\sigma^{\mathrm{A}}(\mathbf{q}, \Omega) = \sigma^{\mathrm{A}}(-\mathbf{q}, -\Omega)$. Here the statistical averaging is performed with the Gaussian complex weight function

$$\mathcal{P}^{\mathrm{A}}_{\mathbf{q},\Omega}(a(\mathbf{q}, \Omega)) = \frac{1}{\pi\sigma^{\mathrm{A}}(\mathbf{q}, \Omega)} \exp\left\{-\frac{|a(\mathbf{q}, \Omega)|^2}{\sigma^{\mathrm{A}}(\mathbf{q}, \Omega)}\right\}. \tag{14}$$

In what follows we assume Gaussian spectral profile of width q_{A} for the ensemble of input images in spatial frequency domain,

$$\sigma^{\mathrm{A}}(\mathbf{q}, \Omega) = (2\pi)^3 \frac{P}{\pi(q_{\mathrm{A}}/2)^2} \exp\left(-\frac{q_x^2 + q_y^2}{(q_{\mathrm{A}}/2)^2}\right) \Pi(\Omega),$$
$$\Pi(\Omega) = \begin{cases} 1/\Omega_{\mathrm{A}}, & |\Omega| \le \Omega_{\mathrm{A}}/2, \\ 0, & |\Omega| > \Omega_{\mathrm{A}}/2, \end{cases} \tag{15}$$

and, for the sake of simplicity, the narrow rectangular spectral profile $\Pi(\Omega)$ of width Ω_{A} and height $1/\Omega_{\mathrm{A}}$ in the temporal frequency domain. Since

$$\sum_{\mathbf{q},\Omega} \sigma_{\mathrm{A}}(\mathbf{q}, \Omega) = L^2 TP, \tag{16}$$

the total average density of photon flux in the image field per $\mathrm{cm}^2\,\mathrm{s}$ is P. The variances of the observables $i_n(\mathbf{q}, \Omega)$ are finally found in the form

$$\left\langle \frac{1}{2}\left\{ i_n(\mathbf{q}, \Omega), i_n^{\dagger}(\mathbf{q}, \Omega)\right\}_+ \right\rangle = B_0^2\left[\sigma_n^{\mathrm{BA}}(\mathbf{q}, \Omega) + \sigma^{\mathrm{A}}(\mathbf{q}, \Omega)\right], \tag{17}$$

where $\{\ ,\ \}_+$ denotes the anticommutator. The quantum noise variances in both detection channels are given by

$$\sigma_n^{\mathrm{BA}}(\mathbf{q}, \Omega) = \left\langle \frac{1}{2}\left\{ f_n(\mathbf{q}, \Omega), f_n^{\dagger}(\mathbf{q}, \Omega)\right\}_+ \right\rangle, \tag{18}$$

$$\sigma_1^{\mathrm{BA}}(\mathbf{q}, \Omega) = \exp[2r_1(\mathbf{q}, \Omega)] \cos^2 \psi_1(\mathbf{q}, \Omega) + \exp[-2r_1(\mathbf{q}, \Omega)] \sin^2 \psi_1(\mathbf{q}, \Omega), \tag{19}$$

$$\sigma_2^{\mathrm{BA}}(\mathbf{q}, \Omega) = \exp[-2r_2(\mathbf{q}, \Omega)] \cos^2 \psi_2(\mathbf{q}, \Omega) + \exp[2r_2(\mathbf{q}, \Omega)] \sin^2 \psi_2(\mathbf{q}, \Omega). \tag{20}$$

Using these results we can evaluate the Shannon mutual information for our dense coding scheme.

3.2 *Shannon mutual information for the spatially-multimode dense coding channel*

It is well known that in the case of a single-mode squeezed light field the statistics of its quadrature amplitudes are Gaussian and can be characterized, e.g. by a Gaussian weight function in the Wigner representation. In the homodyne detection of squeezed light, the statistics of the photocounts are also Gaussian due to the linear relation between the field amplitude and the photocurrent density. Discussion of the homodyne detection in terms of the characteristic function can be found in [15]. Some considerations for the homodyne detection of spatially multimode fields are presented in [10].

In our quantum dense coding scheme the statistically independent degrees of freedom of the noise and the signal are labelled by the frequencies $(\mathbf{q}, \Omega)$ for $\Omega > 0$. One can consider our quantum channel as a collection of the statistically independent parallel Gaussian communication channels in the Fourier domain. The mutual information between Alice and Bob for given detector and frequencies $(\mathbf{q}, \Omega)$ is defined as

$$I_n^{\mathrm{S}}(\mathbf{q}, \Omega) = H_n^{\mathrm{B}}(\mathbf{q}, \Omega) - \overline{H_n^{(\mathrm{B}|\mathrm{A})}(\mathbf{q}, \Omega)}^{\mathrm{A}}. \tag{21}$$

Here $H^{\mathrm{B}}(\mathbf{q}, \Omega)$ is the entropy of Bob's observable and

$$\overline{H_n^{(\mathrm{B}|\mathrm{A})}(\mathbf{q}, \Omega)}^{\mathrm{A}}$$

is the average over the ensemble of the entropy of noise from Alice's signal, introduced by the channel [16]. For the Gaussian channel the mutual information is given by

$$I_n^{\mathrm{S}}(\mathbf{q}, \Omega) = \ln\left(1 + \frac{\sigma^{\mathrm{A}}(\mathbf{q}, \Omega)}{\sigma_n^{\mathrm{BA}}(\mathbf{q}, \Omega}\right). \tag{22}$$

The quantum noise suppression within the frequency range of effective squeezing and entanglement increases the signal-to-noise ratio on the right side of (22). The total mutual information I^{S}, associated with the large area L^2 and the large observation time T, is defined as a sum over all degrees of freedom and is related to the *density of the information stream J in bits per cm*^{2} *s*:

$$I^{\mathrm{S}} = \sum_{n, \mathbf{q}, \Omega > 0} I_n^{\mathrm{S}}(\mathbf{q}, \Omega) = L^2 T J, \tag{23}$$

where

$$J = \frac{1}{(2\pi)^3} \int \mathrm{d}\mathbf{q} \int_{\Omega > 0} \mathrm{d}\Omega \sum_{n=1,2} I_n^{\mathrm{S}}(\mathbf{q}, \Omega). \tag{24}$$

For qualitative and numerical analysis it is natural to associate such quantities as the density of the information stream and of the photon flux with the physical parameters present in our quantum dense coding scheme. Squeezing and entanglement, produced by type-I optical parametric amplifiers (the OPAs), are characterized by the effective spectral widths q_{c} and Ω_{c} in the spatial and temporal frequency domain. The coherence area in the cross-section of the beams and the coherence time are introduced as $S_{\mathrm{c}} = (2\pi/q_{\mathrm{c}})^2$ and $T_{\mathrm{c}} = 2\pi/\Omega_{\mathrm{c}}$. For simplicity, we assume that both OPAs have the same coherence area and coherence time. The correlation area S_{A} and the correlation time T_{A} of non-stationary images, sent by Alice, are related to the spectral widths of the signal q_{A} and Ω_{A} by $S_{\mathrm{A}} = (2\pi/q_{\mathrm{A}})^2$ and $T_{\mathrm{A}} = 2\pi/\Omega_{\mathrm{A}}$. We consider the broadband degenerate collinear phase matching in travelling-wave type-I OPAs. The coherence time T_{c} of the spontaneous down conversion will be typically short compared to the time duration T_{A} of the Alice movie frame.

The dimensionless information stream $\mathcal{J}$ and the dimensionless input photon flux $\mathcal{P}$ are defined by $\mathcal{J} = S_{\mathrm{c}} T_{\mathrm{A}} J$, $\mathcal{P} = S_{\mathrm{c}} T_{\mathrm{A}} P$. That is, we relate both quantities

to the time duration of the Alice movie frame and the coherence area of squeezing and entanglement.

The optimum entanglement conditions in the OPAs are given by

$$\begin{aligned} r_1(\mathbf{q},\Omega) &= r_2(\mathbf{q},\Omega) \equiv r(\mathbf{q},\Omega), \\ \psi_1(\mathbf{q},\Omega) &= \psi_2(\mathbf{q},\Omega) \pm \pi/2 \equiv \psi(\mathbf{q},\Omega), \\ \psi(0,0) &= \pi/2. \end{aligned} \tag{25}$$

We find the dimensionless information stream $\mathcal{J}$ in the following form:

$$\mathcal{J} = \int \mathrm{d}\boldsymbol{\kappa} \ln\left\{1 + \mathcal{P}\frac{1}{\sigma^{\mathrm{BA}}(\boldsymbol{\kappa},0)}\frac{1}{\pi(d_{\mathrm{A}}/2)^2}\exp\left(-\frac{\kappa_x^2+\kappa_y^2}{(d_{\mathrm{A}}/2)^2}\right)\right\}, \tag{26}$$

where

$$\sigma^{\mathrm{BA}}(\boldsymbol{\kappa},0) = \exp\left[2r(\boldsymbol{\kappa},0)\right]\cos^2\psi(\boldsymbol{\kappa},0) + \exp\left[-2r(\boldsymbol{\kappa},0)\right]\sin^2\psi(\boldsymbol{\kappa},0) \tag{27}$$

and the dimensionless spatial frequency is defined as $\boldsymbol{\kappa} = \mathbf{q}/q_{\mathrm{c}}$. The relative spectral width of the Alice signal $d_{\mathrm{A}} = q_{\mathrm{A}}/q_{\mathrm{c}} = (S_{\mathrm{c}}/S_{\mathrm{A}})^{1/2}$ can be interpreted as the number of image elements per coherence length, i.e. the relative linear density of image elements. In what follows we assume a simple estimate $q_{\mathrm{c}}/2 = (2k/l)^{1/2}$, related to the diffraction spread of parametric down conversion light inside the OPA crystal, where k is the wavenumber and l is the crystal length.

Quantum noise in the dense coding scheme is effectively reduced for optimum phase matching of squeezed beams. As shown in [3, 17, 18], an important factor is the spatial-frequency dispersion of squeezing, that is, the **q**-dependence of the phase of the squeezed quadrature component. This dependence is due to the diffraction inside the OPA. A thin lens properly inserted into the light beam can effectively correct the **q**-dependent orientation of squeezing ellipses, as illustrated in figure 2.

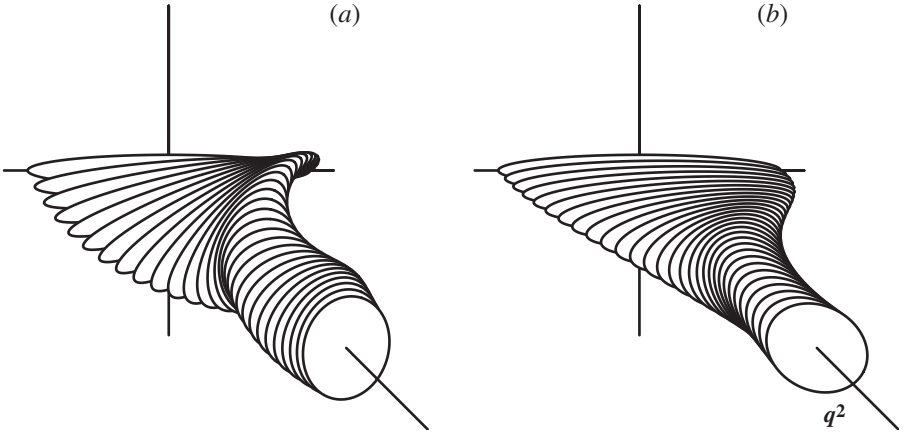

Figure 2. Spatial-frequency dependence of squeezing ellipses (*a*) without and (*b*) with phase correction by means of a thin lens. The degree of squeezing is $\exp\left[r(0,0)\right] = 3$.

The improvement in the signal-to-noise ratio for different spatial frequencies can be characterized by the inverse of the noise variance $\sigma^{\mathrm{BA}}(\boldsymbol{\kappa}, 0)$ shown in figure 3. As seen from this figure, the phase correction by means of a lens allows for the low-noise signal transmission within the spatial-frequency band of the effective squeezing.

In our plots for the mutual information density $\mathcal{J}$ we keep constant the coherence area S_{c}, the degree of squeezing $r(0,0)$, and the density of the signal photon's flux $\mathcal{P}$. The dependence of mutual information density on the relative linear density d_{A} of the image elements is shown in figure 4. For $d_{\mathrm{A}} \ll 1$ (large image elements, $S_{\mathrm{A}} \gg S_{\mathrm{c}}$), the mutual information density increases linearly with d_{A}, since this implies improvement of the spatial resolution in the input signal. In the classical limit (vacuum noise at the input of the scheme), the increase of mutual information density with the density of image elements takes place until the information per Alice's image element becomes of the order or less than one bit:

$$\ln\left\{1 + \frac{4}{\pi}\frac{\mathcal{P}}{d_{\mathrm{A}}^2}\right\} \sim \frac{\mathcal{P}}{d_{\mathrm{A}}^2} \leq 1. \tag{28}$$

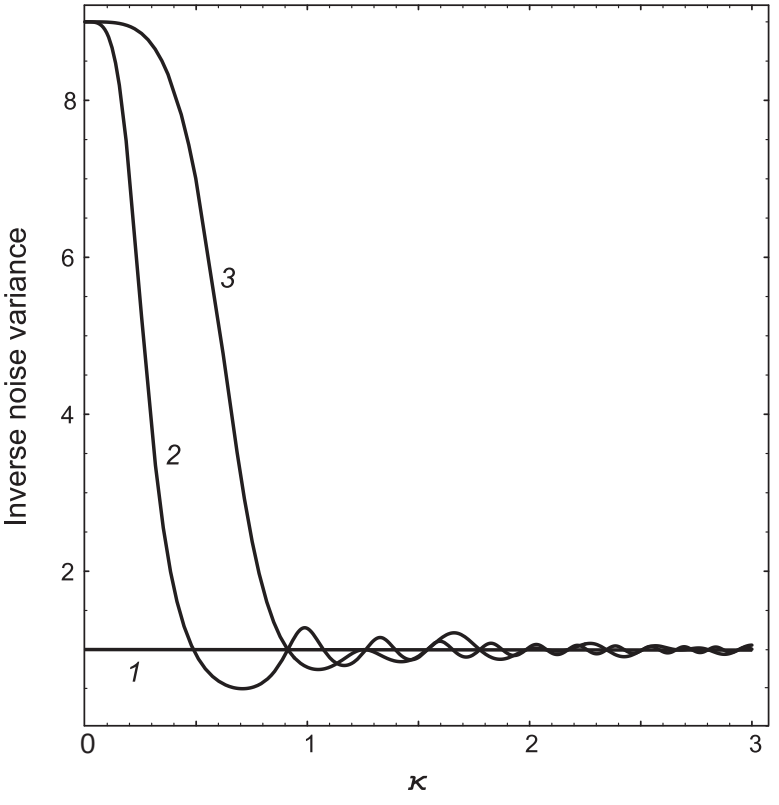

Figure 3. Inverse noise variance with dependence on the spatial frequency κ for vacuum noise at the input (curve 1), and for squeezing with $\exp[r(0,0)] = 3$ without (curve 2) and with (curve 3) phase correction.

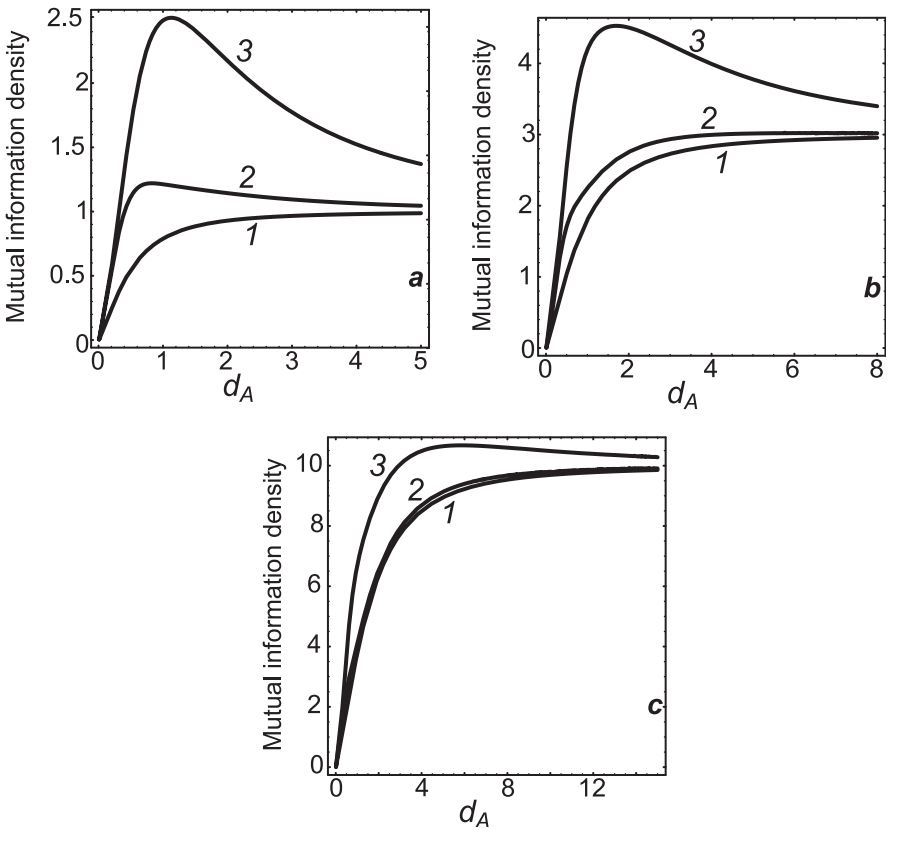

Figure 4. Mutual information density for the vacuum noise at the input of the scheme (curve 1), and for squeezing with $\exp[r(0,0)] = 3$ without (curve 2) and with (curve 3) phase correction. The density of signal photons is (*a*) $\mathcal{P} = 1$, (*b*) $\mathcal{P} = 3$ and (*c*) $\mathcal{P} = 10$.

A further increase of d_A has no effect since it is completely compensated for by the decrease of information per image element. In our plots this corresponds to $d_A \sim \mathcal{P}^{1/2} \sim 1$ for $\mathcal{P} = 1$, $d_A \sim 1.7$ for $\mathcal{P} = 3$, and $d_A \sim 3$ for $\mathcal{P} = 10$ (see figure 4(*a*)–(*c*) correspondingly).

It is instructive to estimate the effect of squeezing and entanglement on the information capacity of our dense coding channel. A standard assumption for such estimate reads,

$$\langle n_{\text{squeezed}} \rangle \sim \langle n_{\text{signal}} \rangle, \tag{29}$$

and implies that the energy costs of squeezing and entanglement (the number of photons in squeezed light per mode at a given detector) are of the order of the signal photon number per mode. Here

$$\langle n_{\text{squeezed}} \rangle = \sinh^2 r \sim \frac{\exp(2r)}{4}. \tag{30}$$

Let us take for simplicity $d_A \sim 1$, when the size S_A of the image element is of the order of the coherence area S_c of squeezed light. Under this condition one can consider the coherence volume $cS_A T_A$ as a degree of freedom for both the signal and the squeezed field. Then

$$\langle n_{\text{signal}} \rangle \sim \mathcal{P} \tag{31}$$

and the assumption (29) means

$$\mathcal{P} \sim \frac{\exp(2r)}{4}. \tag{32}$$

In our plots $\exp(2r) = 9$ and $\mathcal{P} = 1 < \exp(2r)/4$, $\mathcal{P} = 3 \sim \exp(2r)/4$, $\mathcal{P} = 10 > \exp(2r)/4$ in figure 4 (*a*)–(*c*) correspondingly. By inspecting the curves for $d_A \leq 1$ one can observe that for $\langle n_{\text{squeezed}} \rangle \sim \langle n_{\text{signal}} \rangle$ (curves 3 and 1 in figure 4 (*b*)) the information capacity of the dense coding channel exceeds that of the classical channel by a factor of ~ 2.

This result is in agreement with general properties of quantum dense coding, and with the estimate [13] for the single-mode continuous variables scheme.

For $\mathcal{P} < \exp(2r)/4$ (curves 3 and 1 in figure 4 (*a*)) the superiority of the quantum channel is more significant, but in this case the energy costs of squeezing and entanglement exceed the power of the signal itself. The curves 3 and 1 in figure 4 (*c*) illustrate an opposite limit: relatively low energy costs of the quantum channel and a small increase of its information capacity.

For $d_A \gg 1$ (image elements much smaller than the coherence length), the effect of entanglement on the channel capacity is washed out and $\mathcal{J}$ goes down to the vacuum limit. This is due to the fact that in the limit $S_A \ll S_c$ almost all spatial frequencies of the signal are outside the spatial-frequency band of the effective noise suppression, and the channel capacity is finally limited by vacuum noise.

The phase correction of squeezing and entanglement significantly improves the channel capacity, since it brings the spatial frequency band of the effective noise suppression to its optimum value. It eliminates the destructive effect of the amplified (stretched) quadrature of the noise field at the higher spatial frequencies, as seen from figure 4, curves 3 and 2.

4. Conclusion

In this paper we have extended the continuous variables dense coding protocol proposed in [13] onto optical images and calculated the *spatio-temporal density* of the Shannon mutual information. Our multimode quantum communication channel provides much higher channel capacity due to its intrinsic parallel nature. We have considered the role of diffraction in our protocol and have found how to optimize its performance by means of a lens properly inserted into the scheme. We have shown that, by contrast to the classical communication channel, there exists an optimum spatial density of image elements, matched to the spatial-frequency band of squeezing and entanglement.

Acknowledgments

The authors thank L.A. Lugiato and C. Fabre for valuable discussions. This work was supported by the Network QUANTIM (IST-2000-26019) of the European Union, by INTAS under Project 2001-2097, and by the Russian Foundation for Basic Research under Project 03-02-16035. The research was performed within the framework of GDRE 'Lasers et techniques optiques de l'information'.

Appendix: properties of spatially-multimode squeezing

The main results for spatially-multimode squeezing are summarized in [3]. The coefficients of the squeezing transformation (7) satisfy the conditions

$$\begin{aligned} |U_n(\mathbf{q},\Omega)|^2 - |V_n(\mathbf{q},\Omega)|^2 &= 1, \\ U_n(\mathbf{q},\Omega)V_n(-\mathbf{q},-\Omega) &= U_n(-\mathbf{q},-\Omega)V_n(\mathbf{q},\Omega), \end{aligned} \tag{A1}$$

which are necessary and sufficient for preservation of the free-field commutation relations (4). The spatial and temporal parameters of squeezed and entangled light fields essentially depend on the orientation angle $\psi_n(\mathbf{q},\Omega)$ of the major axes of the squeezing ellipses,

$$\psi_n(\mathbf{q},\Omega) = \frac{1}{2}\arg\{U_n(\mathbf{q},\Omega)V_n(-\mathbf{q},-\Omega)\}, \tag{A2}$$

and on the degree of squeezing $r_n(\mathbf{q},\Omega)$,

$$\exp[\pm r_n(\mathbf{q},\Omega)] = |U_n(\mathbf{q},\Omega)| \pm |V_n(\mathbf{q},\Omega)|. \tag{A3}$$

The phase of the amplified quadrature components is given by

$$\phi_n(\mathbf{q},\Omega) = -\frac{1}{2}\arg\{U_n(\mathbf{q},\Omega)V_n^*(-\mathbf{q},-\Omega)\}. \tag{A4}$$

In analogy to the single-mode EPR beams, the multimode EPR beams are created if squeezing in both channels is effective, and the squeezing ellipses are oriented in the orthogonal directions.

For the type-I phase-matched travelling-wave OPAs, the coefficients $U(\mathbf{q},\Omega)$ and $V(\mathbf{q},\Omega)$ are given by

$$\begin{aligned} U(\mathbf{q},\Omega) &= \exp\{\mathrm{i}[(k_z(\mathbf{q},\Omega)-k)l - \delta(\mathbf{q},\Omega)/2]\} \\ &\quad\times\left[\cosh\Gamma(\mathbf{q},\Omega) + \frac{\mathrm{i}\delta(\mathbf{q},\Omega)}{2\Gamma(\mathbf{q},\Omega)}\sinh\Gamma(\mathbf{q},\Omega)\right], \\ V(\mathbf{q},\Omega) &= \exp\{\mathrm{i}[(k_z(\mathbf{q},\Omega)-k)l - \delta(\mathbf{q},\Omega)/2]\}\frac{g}{\Gamma(\mathbf{q},\Omega)}\sinh\Gamma(\mathbf{q},\Omega). \end{aligned} \tag{A5}$$

Here l is the length of the nonlinear crystal, $k_z(\mathbf{q},\Omega)$ is the longitudinal component of the wave vector $\mathbf{k}(\mathbf{q},\Omega)$ for the wave with frequency $\omega+\Omega$ and transverse

component $\mathbf{q}$. The dimensionless mismatch function $\delta(\mathbf{q}, \Omega)$ is given by

$$\delta(\mathbf{q}, \Omega) = \Big(k_z(\mathbf{q}, \Omega) + k_z(-\mathbf{q}, -\Omega) - k_\mathrm{p}\Big)l \approx (2k - k_\mathrm{p})l + k''_\Omega l\Omega^2 - q^2 l/k, \qquad \text{(A6)}$$

where k_p is the wave number of the pump wave, $k_\mathrm{p} - 2k = 0$ in the degenerate case. We have assumed the paraxial approximation. The parameter $\Gamma(\mathbf{q}, \Omega)$ is defined as

$$\Gamma(\mathbf{q}, \Omega) = [g^2 - \delta^2(\mathbf{q}, \Omega)/4]^{1/2}, \qquad \text{(A7)}$$

where g is the dimensionless coupling strength of the nonlinear interaction, taken as real for simplicity. It is proportional to the nonlinear susceptibility, the length of the crystal and the amplitude of the pump field.

References

[1] D. Bouwmeester, A. Eckert and A. Zeilinger (Editors), *The Physics of Quantum Information* (Springer, Berlin, 2000).
[2] S. Braunstein and A. Pati (Editors), *Quantum Information with Continuous Variables* (Kluwer, Dordrecht, 2003).
[3] M.I. Kolobov, Rev. Mod. Phys. **71** 1539 (1999).
[4] L.A. Lugiato, A. Gatti and E. Brambilla, J. Opt. B: Quantum Semiclass. Opt. **4** 176 (2002).
[5] S.L. Braunstein and H.J. Kimble, Phys. Rev. Lett. **80** 869 (1998).
[6] D. Bouwmeester, J.-W. Pan, K. Mattle, *et al.*, Nature (London) **390** 575 (1997); D. Boschi, S. Branca, F. De Martini, *et al.*, Phys. Rev. Lett. **80** 1121 (1998).
[7] A. Furusawa, J.L. Sorensen, S.L. Braunstein, *et al.*, Science **282** 706 (1998).
[8] W.P. Bowen, N. Treps, B.C. Buchler, *et al.*, Phys. Rev. A **67** 032302 (2003).
[9] I.V. Sokolov, M.I. Kolobov, A. Gatti, *et al.*, Opt. Commun. **193** 175 (2001).
[10] A. Gatti, I.V. Sokolov, M.I. Kolobov, *et al.*, Eur. Phys. J. D **30** 123 (2004).
[11] C.H. Bennett and S.J. Wiesner, Phys. Rev. Lett. **69** 2881 (1992).
[12] K. Mattle, H. Weinfurter, P.G. Kwiat, *et al.*, Phys. Rev. Lett. **76** 4656 (1996).
[13] S.L. Braunstein and H.J. Kimble, Phys. Rev. A **61** 042302 (2000).
[14] X.Y. Li, Q. Pan, J. Jinq, *et al.*, Phys. Rev. Lett. **88** 047904 (2002).
[15] S.L. Braunstein, Phys. Rev. A **42** 474 (1990).
[16] A.S. Holevo, *Probabilistic and Statistical Aspects of Quantum Theory* (North-Holland, Amsterdam, 1982).
[17] M.I. Kolobov and I.V. Sokolov, Sov. Phys. JETP **69** 1097 (1989).
[18] M.I. Kolobov and I.V. Sokolov, Phys. Lett. A **140** 101 (1989).